Journal of Materials Chemistry A

Accepted Manuscript

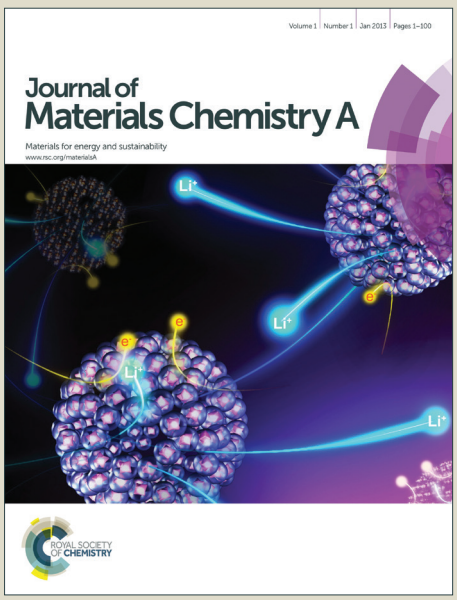

ROYAL SOCIETY OF CHEMISTRY

www.rsc.org/materialsA

Journal Name

ARTICLE

Recent Progress in Photocathodes for Hydrogen Evolution

Qiang Huang[a,b,c], Zi Ye[b], Xudong Xiao[b,*]

Received 00th January 20xx,
Accepted 00th January 20xx

DOI: 10.1039/x0xx00000x

www.rsc.org/

Solar water splitting, which has been a topic of intensive research interest for several decades, is one of the promising approaches to utilize renewable energy to maintain the sustainable prosperity of our society. However, up to now no mature photoelectrochemical cell can be used in practical large-scale applications because of the difficulties to satisfy all the harsh requirements, including high energy conversion efficiency, high stability and low cost. This feature article reviews the recent progress in developing photocathodes in photoelectrochemical cell for solar hydrogen production. Both the developments of the p-type semiconductor light absorbers and the efforts to develop synergistic approaches to improve the overall performance of the photocathode are discussed.

Introduction

As the worldwide convertible currency of industry and daily life, energy is a critical foundation for economic growth and social progress. Since the beginning of the industrial revolution, fossil fuels, such as coal, oil and natural gas, have supplied the main energy demand. However, as a result of the rapid global economic development and rural urbanization[1, 2], the energy consumption grew tremendously fast and now we are facing more and more serious shortage of the traditional fossil fuels. For example, the world crude oil production rate has outstripped its discovery rate since 1980s, which will cause the decrease of the overall oil production after 2030[3]. In fact, energy was selected as the single most important factor that impacts the sustainable prosperity of our society[4]. On the other hand, the emissions of the greenhouse gases, such as the CO_2, are associated with the traditional hydrocarbon fuel combustions and raise worldwide concerns about their impact on climate change. To weasel out of this predicament, alternative carbon-free energy options, such as solar, nuclear, wind, geothermal, hydroelectric, and biomass have been sought to fulfill the global energy demand to maintain both the rapid economy growth and the sustainable environmental protection[5]. Though the fossil fuels will still dominate the energy production in the next 40 years, the renewable sources are predicated to provide up to 90% of the total energy by the end of this century. Among them, solar energy has the largest potential of large-scale application, which will take up about 65% of the total energy supply[6]. After all, the solar energy strikes the earth with about 180 000 TW of radiant power and can provide enough energy for our present annual energy consumption (~ 17 TW) in just about one hour[7, 8].

The solar energy could be utilized by several different strategies, such as solar to electricity conversion via photovoltaic cells, solar to thermal conversion with concentrated sunlight heat-engines or solar water heaters, solar to fuel conversion with solar water splitting cells and so on. Among all these methods, solar to hydrogen conversion is very promising because of the carbon-free and high gravimetric energy (143 MJ/kg) characteristics of hydrogen, which is an excellent energy carrier for the intermittent solar energy and can be directly used as a fuel in an engine or fuel cell[9]. In fact, direct photo-reduction of water into hydrogen by semiconductors has attracted great attention because of its advantage of using only water and sunlight, both of which are widely distributed, as raw materials[10-12].

The solar hydrogen production has been a topic of intense research interest for more than 40 years. Since the discovery by Fujishima and Honda[13], who used TiO_2 photoelectrode to demonstrate the solar water splitting process, many materials have been extensively investigated in order to achieve the efficiency that could be commercialized for practical use. Now there are two types of cell configurations for solar water splitting: one is the colloidal configuration (photocatalyst cell) and the other is the photoelectrode configuration (photoelectrolysis cell)[14, 15]. In the colloidal configuration, photocatalyst particles are suspended in the electrolyte, and each particle usually has active sites for both the water reduction and water oxidation. In the photoelectrode configuration the semiconductor materials for light absorption are immobilized to be an electrode on which half of the water redox reaction takes place, while the other half reaction usually occurs at the counter electrode (prepared either using metal or other semiconductor materials) connected via an external circuit. Generally speaking, the photoelectrolysis cell could automatically separate the hydrogen evolution sites

[a] Center of Interface Dynamics for Sustainability, China Academy of Engineering Physics, Chengdu, Sichuan 610200, China.
[b] Department of Physics, The Chinese University of Hong Kong, Shatin, New Territory, Hong Kong, China.
[c] Science and Technology on Surface Physics and Chemistry Laboratory, P.O. Box 718-35, Mianyang 621907, Sichuan， China
DOI: 10.1039/x0xx00000x

from that of oxygen and enable the photoelectrochemical investigation of materials more easily.

The major component of the photoelectrolysis cell, or the photoelectrochemical (PEC) cell, is the photoanode, photocathode or both, and there are many previous reviews for the photoanode and the overall solar water splitting cell[16-25]. In this feature article, we will focus on providing an overview on the recent efforts in developing photocathodes for solar hydrogen evolution. After a brief introduction of the principles for the photoelectrolysis cell, the materials recently investigated for photocathode will be reviewed, together with the overview of several approaches used to improve the performance, such as the activity and stability. Finally, the challenges and perspectives in this filed will be addressed.

Principles of photoelectrolysis cell

Overall solar water splitting

The solar water splitting principle can be briefly described by Fig. 1(a). The photo-excited electrons and holes, which are produced (step (1)) in the photoelectrode by absorbing the photons with proper energy, are transferred (step (2)) to the photoelectrode/electrolyte interface to reduce/oxidize (step (3)) water into hydrogen/oxygen respectively. The photoelectrode material should have appropriate valence/conduction band edges for straddling the water

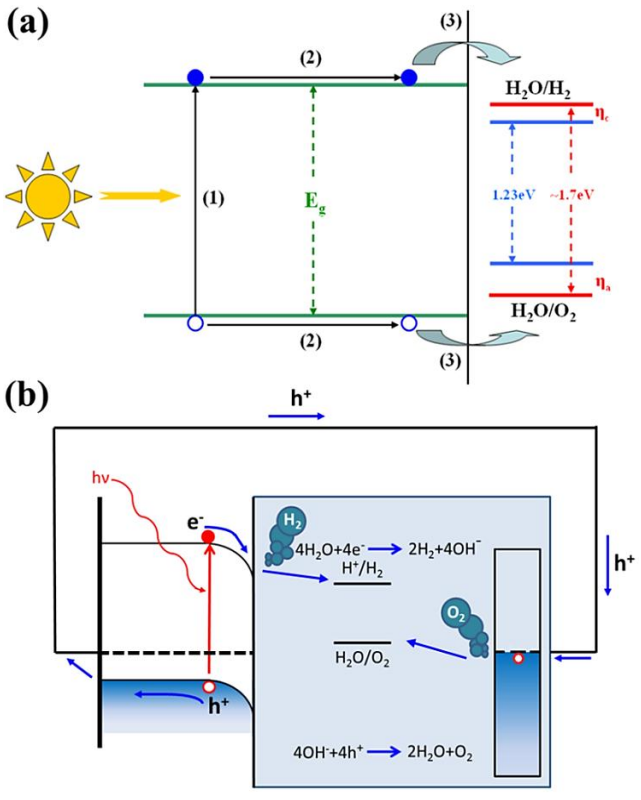

Fig.1 (a) The overall solar water splitting process at the semiconductor photoelectrode illuminated by sunlight. (b) Energy diagram of the photoelectrochemical cell based on photocathode under illumination.

oxidation/reduction potential levels to split water without external bias. Using one single semiconductor to achieve the overall solar water splitting, the bandgap should be about 1.7 eV after considering the overpotentials for both the hydrogen evolution (η_c) and the oxygen evolution (η_a). This bandgap is higher than the water decomposition energy of 1.23 eV calculated from the standard Gibbs free energy[21]. However, up to now there is no robust photoelectrode material that could be used for the overall water splitting with promising energy conversion efficiency and fabrication cost, and much attention has been paid to study the two half-reactions of water splitting on photoanode and photocathode respectively.

Photocathode for hydrogen evolution

The photoanodes usually suffer significant photo-corrosion due to their self-photo-oxidation at the photoelectrode/electrolyte interface by the photo-excited holes, and scavengers, such as S^{2-} and SO_3^{2-}, are required to prevent this photo-corrosion. In comparison, the photocathodes based on p-type semiconductors are reported to be cathodically protected from this photo-oxidation, making them expected to be more stable than the photoanodes[10, 21]. In this case, the photo-generated electrons will migrate to the photocathode/electrolyte interface and the excited holes will transport to the counter anode through external wire circuit or with wireless contact, which is facilitated by the band bending at the interface due to the space charge effects as shown in Fig.1(b)[11, 26]. To achieve the hydrogen evolution at the photocathode/electrolyte interface, the conduction band edge of the photocathode material should be more negative than the water reduction potential level in the normal hydrogen electrode (NHE) scale. The scope of this article will be focused on the recent research progress of photocathode, which can be combined with a counterpart-an anode to realize the whole water splitting reaction.

Photocathode materials

There are several main challenges for the semiconductor materials to be used for fabricating the practical photocathodes. Firstly, the conduction band edge of the semiconductor should be more negative in NHE than the hydrogen evolution potential level considering the corresponding overpotential. The photo-voltage, which is related to the bandgap, should be as large as possible to avoid using external bias or to release the constraint on the material selection for the counter anode. Fig. 2 shows the overview of the energy positions of conduction band edge (CB) and valence band edge (VB) for several photocathode semiconductors. Secondly, the semiconductor should be visible-light responsive to make best use of the solar radiation in order to increase the solar energy conversion efficiency as high as possible. Taking CdS (2.42 eV), Cu_2O (2 eV) and $CuGaSe_2$ (1.7 eV) as examples, their theoretical upper limits of conversion efficiency are 9%, 18% and 27.8% respectively (Fig.3). Thirdly, the material must

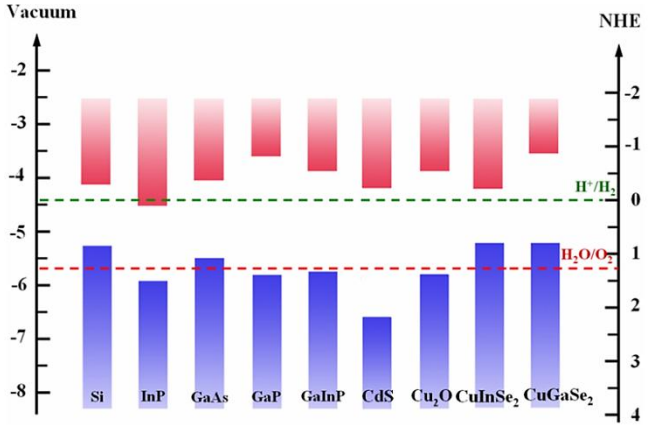

Fig.2. Overview of the energy positions of conduction band edge and valence band edge for several photocathode semiconductors. Also shown as the dashed lines are the water oxidation/reduction potential levels[18, 27-32].

be stable in aqueous electrolyte under illumination to ensure long lifetime. The last one but not an unimportant one is that the material should be earth abundant to guarantee both the high performance/price ratio and the feasibility of wide application. The rarest elements should not be used as light absorbers in solar water splitting system, while minute quantities of them used as catalysts may be affordable such as the industrial application of Pt in fuel cell and exhaust gas treatment system. To date there is no material found to handle all these challenges well, although intensive research has been carried out.

The following reviews the recent progress of the photocathode materials which are divided into several groups including metal oxides, III-V group materials, Si, copper-based chalcogenides, and II-VI group materials.

Metal oxides

Compared to the non-oxide counterparts, the metal oxide semiconductors usually have the advantage of simple synthesis procedure. As a result of the intrinsic oxygen vacancies defects (V_O) acting as electron donors, the metal oxide semiconductors, such as Fe_2O_3 (2.2 eV), WO_3 (2.6 eV), and $BiVO_4$ (2.4 eV), are generally n-type conduction materials and are used as photoanodes. Distinctively, several metal oxide semiconductors, such as binary oxide Cu_2O (2.0 eV), ternary oxides $CaFe_2O_4$ (1.9 eV), $CuNb_3O_8$ (1.5 eV), $CuFeO_2$ (1.5eV), and $LaFeO_3$, are dominated by the metal vacancies defects (V_M) to show p-type conductivity and thus can be investigated as photocathodes [33-41]. In fact, although metal oxides often meet the criteria with regard to the chemical stability and low cost, they usually have modest optical absorption coefficients, poor charge-carrier mobility and short charge-carrier lifetime. Therefore, the resultant photocurrent and energy conversion efficiency remain low.

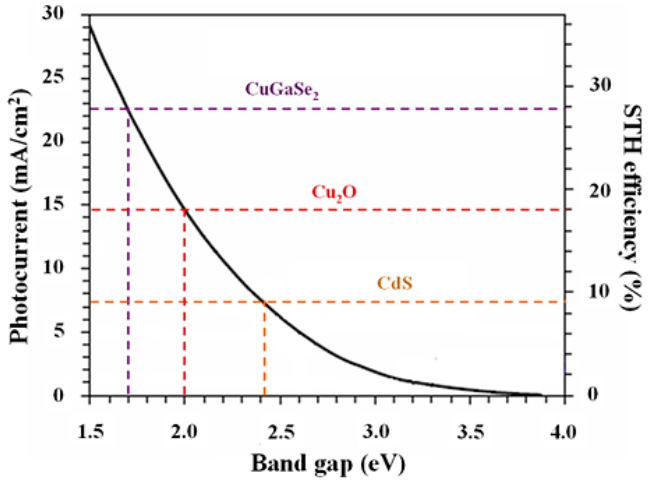

Fig. 3 The relation between the semiconductor bandgap and the theoretical photocurrent under AM 1.5G illumination and solar to hydrogen (STH) conversion efficiency[27-29].

As a simple p-type oxide semiconductor with a theoretical 18% solar-to-fuel conversion efficiency (Fig.3), Cu_2O is now attracting more and more attention. Previous studies reported that the band edges of Cu_2O can straddle the water reduction and oxidation potential levels[27]. The conduction band of Cu_2O is 0.7 eV more negative in NHE than the hydrogen evolution potential and the valence band is just slightly more positive than the oxygen evolution potential[42]. Thus, a relative large driven force to hydrogen evolution reaction from Cu_2O can be expected. With the direct bandgap of 1.9 to 2.2 eV, Cu_2O can well absorb the visible light of solar spectrum[43]. These features make Cu_2O to be a potential photocathode to achieve overall water splitting with no external bias. Unfortunately, the potential levels for the self-reduction from Cu_2O to Cu (Eq. 1) and self-oxidation to CuO (Eq. 2) are all within the bandgap[44], which limit the stability of Cu_2O in aqueous solution and thus the energy conversion efficiency improvement. Nevertheless, many efforts, such as optimizing crystal orientation, surface modification, and nanostructure design, have been made to improve the stability of Cu_2O in the last years.

$$2\mathrm{CuO} + \mathrm{H_2O} + 2e^+ \rightarrow Cu_2O + 2OH^- \qquad \text{Eq. 1}$$
$$Cu_2O + \mathrm{H_2O} + 2h^+ \rightarrow 2\mathrm{CuO} + 2H^+ \qquad \text{Eq. 2}$$

Diverse methods have been explored to produce Cu_2O films. The electrodeposition is preferred due to its relative low cost and ease control of morphology, structure and orientation[45]. A number of studies have been devoted to illustrate the relationship between the crystal orientations and the stability of Cu_2O made by electrodeposition[39, 43, 46]. By controlling the deposition conditions, Sowers *et al.* revealed that the predominated Cu^+ terminated (111) surface in polycrystalline Cu_2O is more stable than other orientations against reduction under illumination[39, 47]. In the opposite, the single crystal of (211) or (311) with O^{2-} terminated surface has been proven unstable[48]. Thus, Cu_2O films with predominated Cu^+ termination degrade not as fast as films with predominated O^{2-} termination. These explorations on mechanisms about how the crystal structure influences the stability of Cu_2O suggest that a controllable stability can be achieved.

Besides optimizing the Cu_2O structure, recently there are many works focus on building the protecting heterojunction layer. In terms of the photoelectrolysis, heterojunction structures have several advantages, such as holding multiple band gaps for matching the solar spectrum, improving the catalytic activity of the photoelectrode surface, passivating the surface to reduce the carrier recombination and enhance the chemical stabilization[21, 49, 50]. For Cu_2O photocathode, the main issue in the heterojunction layer design is to protect Cu_2O from self-reduction while ensuring good charge transfer, which means that an aqueous solution-stable material with suitable band structure is required. One example is given by Paracchino *et al.*[27], using atomic layer deposition (ALD) to grow an Al:ZnO/TiO_2 bi-layers on top of the Cu_2O photocathode (Fig.4(a)). They finally obtained a photocurrent density up to 7.6 mA/cm^2 at 0V vs RHE (reversible hydrogen electrode, a subtype of the standard hydrogen electrodes for electrochemical processes) under AM 1.5G illumination (Fig.4 (b)), the highest ever for an oxide-based photocathode. Here,

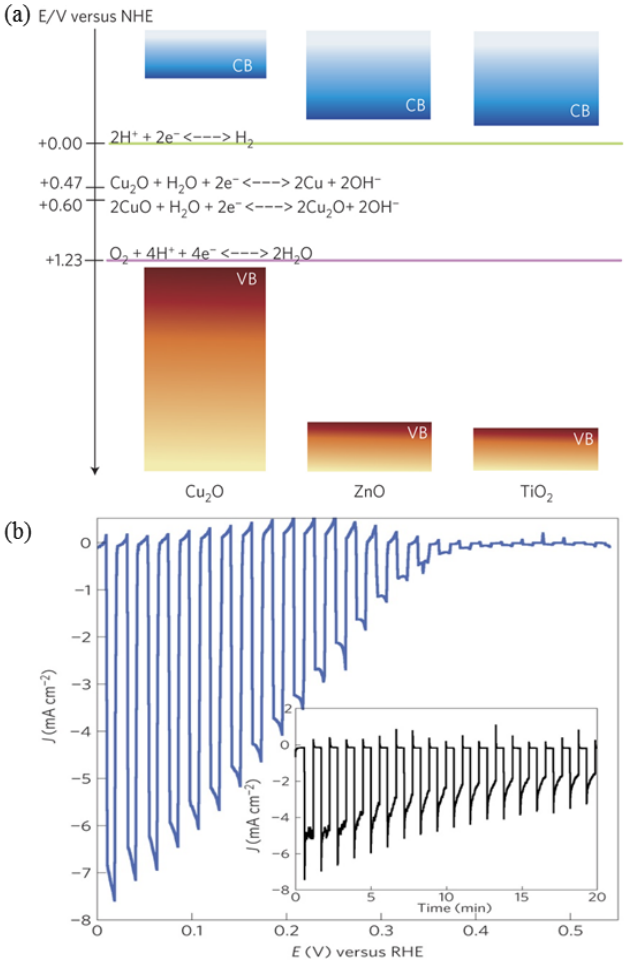

Fig. 4 (a) Energy band positions of the semiconductors used in the multilayered photocathode. The redox levels of the involved chemical reactions are also shown. (b) Current–potential characteristics in 1M Na2SO4 solution, under chopped AM 1.5G light illumination for the as-deposited Cu2O/Al:ZnO/TiO2/Pt. The inset show the photocurrent transients for the electrodes held at 0V vs RHE in chopped light illumination with N2 purging[27]. Copyright 2011 Macmillan Publishers Limited.

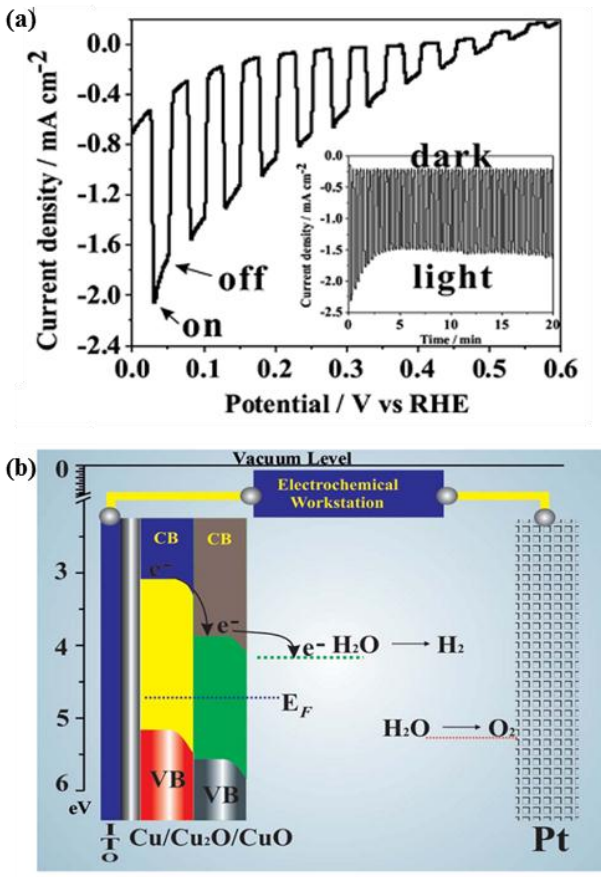

Fig. 5 (a) Photoelectrochemical response of the Cu/Cu_2O/CuO photoelectrode under illumination of chopped AM 1.5G. The inset shows the photocurrent density decay for the electrode held at 0 V vs RHE under chopped light illumination. (b)Proposed energy band diagram of the Cu/Cu_2O/CuO composite electrode.[45] Copyright 2012 The Royal Society of Chemistry.

the suitable conduction band position of ZnO and TiO_2 enable the photo-generated electrons to flow from the Cu_2O automatically to the electrolyte. The thin Al:ZnO buffer layer which is applied in many other photovoltaic devices avoids the reduction of Cu_2O at pinholes of TiO_2 and forms a p-n junction with Cu_2O to promote electron-hole separation [27, 46, 51]. However, because of the Ti^{3+} (electron traps) in TiO_2 film and low driving force for electron injection into electrolyte, the photocurrent degrades substantially even in a 20 minutes of testing. Using the remnant ratio of photocurrent, the ratio of the photocurrent density at the end of the last light cycle to that at the end of the first light cycle, to characterize the stability of the photoelectrode, these authors have improved the stability to a remnant ratio of 62% over 10 hours of testing through the deposition of a semi-crystalline TiO_2 overlayer onto Cu_2O/Al:ZnO by controlling the ALD deposition temperature and selecting suitable electrolyte[51].

Another material used for developing the heterojunction is CuO. In 2009, Zhang and Wang prepared a copper oxide composite photocathode (Cu_2O/CuO) through electrochemical deposition[45]. Twice as much photocurrent (1.54 mA/cm^2, see Fig. 5(a)) as that from bare Cu_2O electrode is achieved when

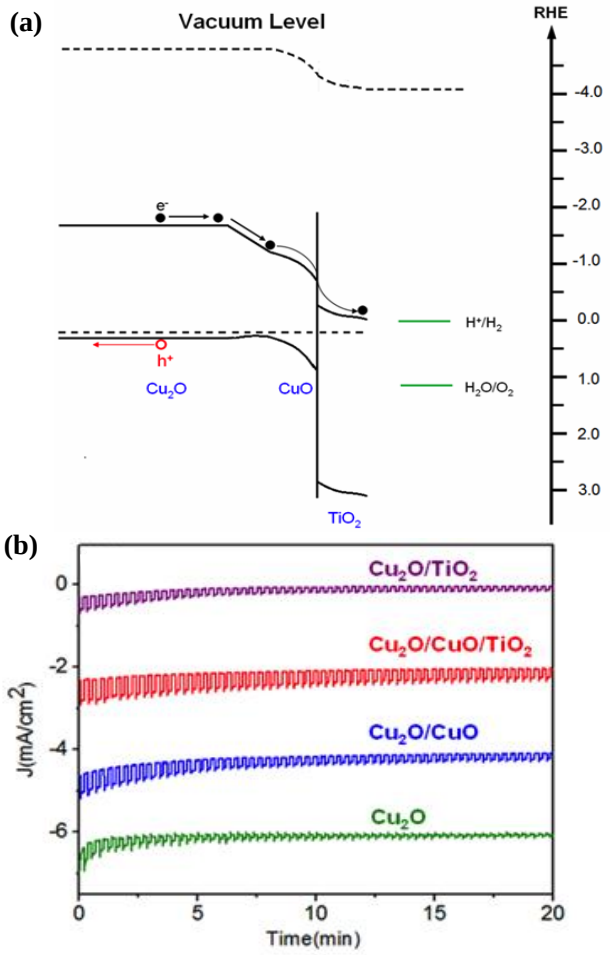

Fig. 6 (a) Energy band diagram of $Cu_2O/CuO/TiO_2$ in 1.0 M Na_2SO_4 electrolyte in the dark. (b) Current–time curves of different nanowire arrays held at 0 V vs RHE under chopped light illumination for stability test. The curves of bare Cu_2O (green line), Cu_2O/CuO (blue line) and $Cu_2O/CuO/TiO_2$ (red line) are shifted vertically for clarity[32]. Copyright 2013 The Royal Society of Chemistry.

measured at a potential of 0 V vs RHE at a mild pH under illumination of AM 1.5G. The remnant ratio of photocurrent after 20 minutes testing was improved from 30.1% to 74.4%. In this structure, CuO as an indirect band gap semiconductor with relative low recombination rate has a good band alignment with Cu_2O (Fig. 5(b)). The photo-generated electrons from Cu_2O can easily transfer to the electrolytes through CuO while the hole transportation is hindered without phonon assisting. Besides the traditional ways to grow Cu_2O/CuO, Han *et al.* developed an easy method to build Cu_2O/CuO heterojunction by fast annealing of a copper foil in H_2–O_2 flame[52]. In such way, a junction is formed between CuO(110) and Cu_2O(111), which again exhibits a better PEC performance than the bare Cu_2O photocathode.

Based on the idea of heterojunction construction, nanomaterials with special shapes, such as nanowires and nanorods which can reduce the diffusion distance for the photo-excited charge carriers to transfer from the generation position to the photoelectrode/electrolyte interface, are used to improve the performance of heterojunction structured photoelectrode. Although the diffusion length of the minority carriers (electrons) in Cu_2O film (less than 100 nm) is not compatible with the absorption length of light (i.e., 2.2 μm), photocathode with highly aligned Cu_2O nanowire arrays offers the possibility to accommodate this problem well and is expected to produce much higher photocurrent than that of the planar Cu_2O photocathode[32, 46]. By fabricating highly aligned $Cu_2O/CuO/TiO_2$ nanowire arrays on Au substrate, indeed the photoresponse and stability of Cu_2O was much improved by the outer CuO/TiO_2 bi-layers (Fig.6a)[46]. The photocurrent increased from 0.45 mA/cm^2 for Cu_2O nanowire arrays to 0.84 mA/cm^2 for $Cu_2O/CuO/TiO_2$ nanowire arrays (Fig.6b) and the remnant ratio of photocurrent after a 20 minute testing also increased to 44%.

Incorporation of co-catalyst or plasmonic effect on the surface of photoelectrode is also used to enhance the PEC performance of copper oxides. To distinguish from the photocatalyst (suspended colloidal particles in solution), the catalyst used to assist the light absorbers in accomplishing the full water redox reaction is usually termed as co-catalyst. Pt, which has played an important catalytic role in many fields, such as the fuel cell technology, automotive emission control, and artificial fuel generation[53-56], is frequently used as a co-catalyst in water splitting. Other noble metals, such as Ru and Pd, have also been extensively investigated as co-catalysts on photoelectrodes. Guo *et al.* reported the deposition of Pd on CuO via photo-assisted electrodeposition enhanced the photocurrent through lowering the overpotential of hydrogen production and accelerating the electron transportation[57]. MoS_{2+x} was also investigated as a co-catalyst for Cu_2O photocathode[58, 59]. Morales-Guio *et al.* first reported that amorphous MoS_{2+x} as a co-catalyst on $Cu_2O/Al:ZnO/TiO_2$ electrode exhibited a photocurrent as high as 6.3mA/cm^2 at 0V vs RHE, which opened a new way for the application of earth abundant catalyst materials in basic electrolysis[58]. Besides Cu_2O, CuO is also used as photocathode. Recently, Zhao *et al.* reported that for the CuO nanowire arrays photocathode a four-fold photocurrent enhancement was produced after being decorated with Ag nanoparticles of average diameter of ~85 nm, now due to the enhanced energy transfer from metal to semiconductor by surface plasmon resonance effect[60].

Besides the binary metal oxide, ternary complex metal oxides offer new choices for photocathode. One example is the p-type $CaFe_2O_4$. Ida have investigated $CaFe_2O_4$ as photocathode material and hydrogen gas was evolved from its surface without any external voltage bias when being used together with a TiO_2 photoanode[61]. More impressively, $CaFe_2O_4$ photocathode with metal doping shows a much higher photocurrent due to the expansion of the absorption wavelength range, the plasmon resonance effect, and the release of structure distortion after doping Ag in $CaFe_2O_4$ structure (Fig.7)[62]. Another example is Cu(I)-niobate system. Joshi and Maggard reported $CuNb_xO_y$ series films such as

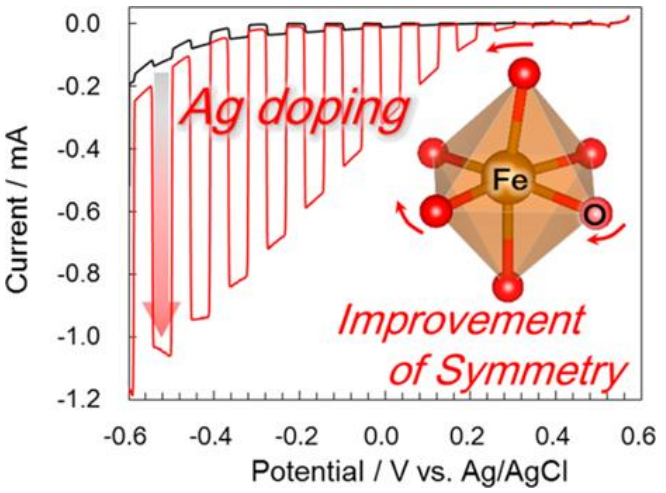

Fig. 7 Current–potential characteristics of Ag doped p-type $CaFe_2O_4$ photocathode (red line) and of undoped $CaFe_2O_4$ photocathode (black line)[62]. Copyright 2014 American Chemical Society.

$CuNbO_3$ with a band gap of 2.0 eV and $CuNb_3O_8$ with a smaller band gap. Through the intentional bandgap design, for $CuNb_3O_8$ which possesses a suitable conduction band for visible-light response, a cathodic photocurrent under visible-light irradiation with incident photon to current efficiency up to ~6-7% and a Faradic efficiency of ~62% were achieved[36]. The Cu(I)-tantalate system including $Cu_2Ta_4O_{11}$,[20, 63] $Cu_3Ta_7O_{19}$, and $Cu_5Ta_{11}O_{30}$[64] has a relatively smaller range of bandgap from 2.4 to 2.6 eV and also exhibits high cathodic photocurrents in aqueous solutions under visible-light irradiation[64].

III-V group materials

In the non-metal oxide semiconductors, III-V materials with relative narrow bandgap have shown high photo-response activity. These materials can be divided into binary compounds such as InP, GaP and ternary compounds such as GaInP[65], GaInN[66] and AlGaAs[67]. Recently, III-V materials such as GaP (2.2 eV) and InP (1.34 eV) were utilized to split water with the assistance of external voltage bias[68-70].

Despite GaP has large photo-voltage, the large planar structure not only is expensive but also limit the charge collection. Nano-texturing the GaP material is preferred in order to promote the charge separation and lower the overpotential[71, 72]. P. D. Yang's group reported a photocathode based on Zn doped GaP nanowires via solution-liquid-solid method. With only 1/3000 of the amount of material used in the planar structure, the electrode showed a photocurrent density of about 0.1 mA/cm^2 at 0V vs RHE under AM 1.5G illumination[68]. Assisted by Ru contained co-catalyst, Lee *et al.* reported that a p-type InP nanopillar photocathode prepared by simple self-masking reactive ion etching process could achieve 14% energy conversion efficiency[69]. In their nanotextured structure, TiO_2 acted as a passivation layer co-operated with the Ru co-catalyst to enhance the photocathode stability. Compared to planar structure, nanotextured structure lowers the surface energy of hydrogen desorption and improves the PEC performance. However, the usage of the corrosive electrolyte and the necessary bias hindered its wide application[69]. Gao *et al.* also fabricated vertically aligned p-type InP nanowire arrays with noble-metal-free MoS_3 nanoparticles as co-catalyst. Compared to noble metal co-catalyst, the photocathode efficiency after adding MoS_3 is improved to 6.4% under AM 1.5G illumination with only 3% of the surface area covered by InP nanowires (Fig.8) [70].

$GaInP_2$ is an example of ternary compounds. p-type $GaInP_2$ with a band gap in the ideal range (1.8 to 1.9 eV) can serve as a photocathode, although the energetics of its band edges are not well aligned with water redox potential levels and requires an additional 300 mV voltage bias for water splitting[73]. Khaselev and Turner designed a p-n GaAs/p-n tunnel junction/$GaInP_2$/Pt tandem cell which reached a 12.4 % energy conversion efficiency and stimulated the worldwide great interest[10]. In this configuration, the visible light responsive $GaInP_2$ (1.83 eV) top photocathode was internally biased by near-infrared light responsive bottom GaAs (1.42 eV) p-n junction cell through a tunneling diode interconnection (Fig.9(a)). The GaAs bottom cell effectively supplied an internal voltage bias to make up the energy band mismatch to overcome the energy difference from hydrogen evolution reaction. This device combined GaAs and $GaInP_2$ to drive the charge separation and split water directly under illumination without external bias (Fig.9(b)). Later, Licht *et al.* further improved the device and demonstrated 18.3 % energy conversion efficiency[67]. Similarly, $Al_{0.15}Ga_{0.85}As$ (1.6 eV) and Si (1.1 eV) together can form a stacked multi-junction structure and has reached high energy conversion efficiency when catalyzed by RuO_2. On the one hand, the extremely expensive cost of the raw materials and fabrication procedures made this

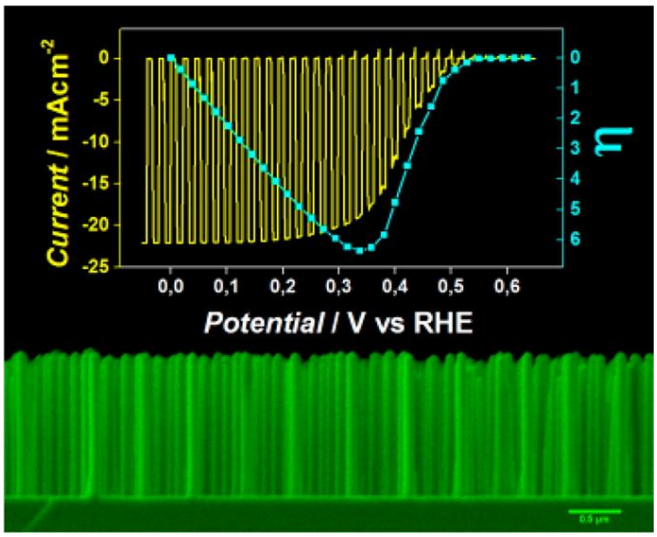

Fig. 8 Current–potential curves (yellow solid line) and photocathode energy conversion efficiencies (blue squares) of the as-grown InP nanowire arrays with MoS_3 co-catalyst in 1M $HClO_4$ under chopped AM 1.5G illumination[70]. Copyright 2014 American Chemical Society.

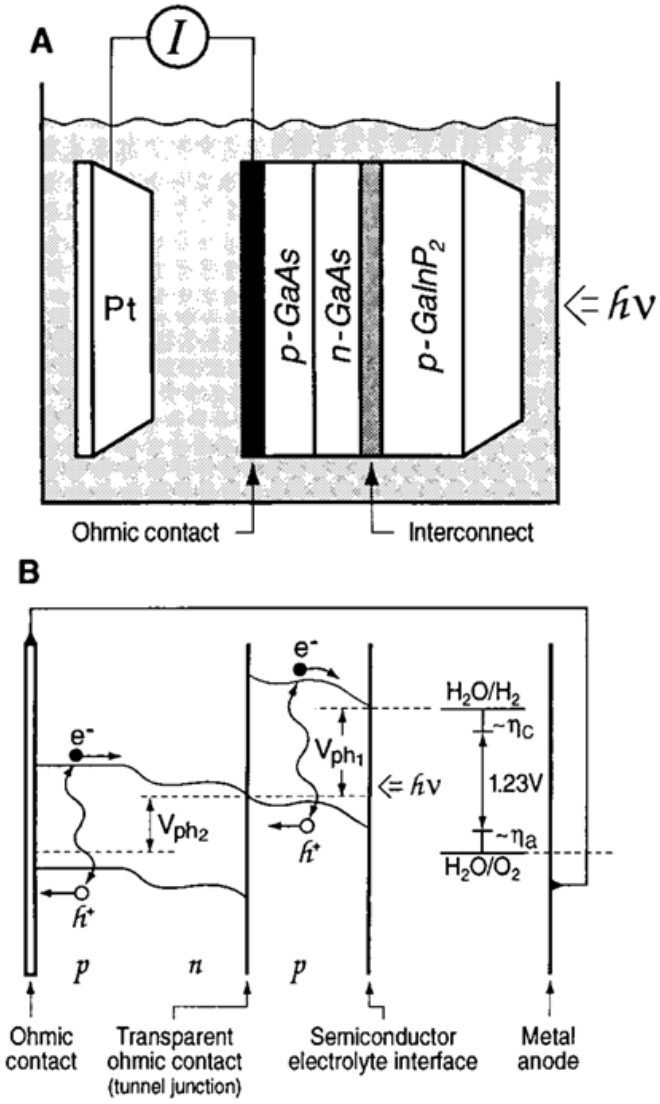

Fig.9 (a) Schematic of the p-n GaAs/p-n tunnel junction/p-$GaInP_2$ tandem PV/PEC cell. (b) Idealized energy level diagram for the p-n GaAs/p-n tunnel junction/p-$GaInP_2$(Pt) electrode.[10] Copyright 1998 the American Association for the Advancement of Science.

kind of structure not cost competitive, despite of the demonstrated industry scale efficiency over 10%. On the other hand, the current mismatch between different layers still limited the performance. Thus, Fan *et al.* recently exploited a lateral carrier extraction scheme of one-dimensional nanowire structures, consisting of n-GaN/tunnel junction/p-InGaN nanowire arrays and a Si solar cell wafer, without strict current matching requirement[74]. The monolithically integrated photocathode exhibited a photon-to-current efficiency of 8.7% at an bias voltage of 0.33 V vs RHE[74]. Wu *et al.* reported that InGaP passivated GaAsP nanowires showed better photoluminescence than the unpassivated one because of the reduced density of surface trapping sites and the increased charge carrier confinement after passivation.[75]

Silicon

Up to now, silicon is the most widely used semiconductor for solar energy conversion because of its earth abundance and its prevalence in industry. Besides its application in photovoltaic solar cells, p-Si is a promising photocathode because of its appropriate conduction band edge for hydrogen evolution. With a small bandgap (~1.1eV), its valence band edge is much lower in NRE than the oxygen evolution potential level and therefore it requires an n-type photoanode to work together to achieve overall water splitting. However, low stability from etching or oxidizing in electrolyte as well as no effective surface co-catalysts are the main reasons hindering the performance of Si photocathode.

For the planar silicon structure, earlier works have used metal catalyst such as Pt[76], Ni and Ni-Mo[77] to lower the overpotential to efficiently transfer photo-charges for hydrogen evolution. Recently, cheap non-metal co-catalysts MoS_2[78], TiO_2[79], NiO_x[80] and Al_2O_3[81] are widely used as a surface protection layer in the PEC cell and are applied on the p-Si photocathode. Benck *et al.* deposited a thin layer MoS_2 onto n^+p planar Si photocathode (**Fig. 10**) to achieve over 100 hours stability in electrolyte[78]. Moreover, Ding *et al.* demonstrated exfoliated MoS_2 covered planar p-Si as efficient photocathode for hydrogen evolution[82]. With n-butyl lithium (n-BuLi) treatment, the semiconducting 2H-MoS_2 phase is converted into metallic 1T-MoS_2 phase and can accommodate more facile electrode kinetics. 1T-MoS_2 made an invertible and fast electron transfer, while the holes were left in Si. Thus, a photocurrent up to 17.6 mA/cm^2 at 0 V vs RHE under AM 1.5G illumination was achieved in this fast charge separation and slow charge recombination structure. With the protection of MoS_2 layer, 1T-MoS_2/Si photocathode was monitored periodically over 70 days, and no noticeable degradation in performance was observed.

The Si wire structure is widely used in recent years. Because of the indirect bandgap of Si and the resultant large absorption length, nearly a 200 μm thickness is required for planar structure. In the wire structure, separation between the absorption length of light and the collection length of

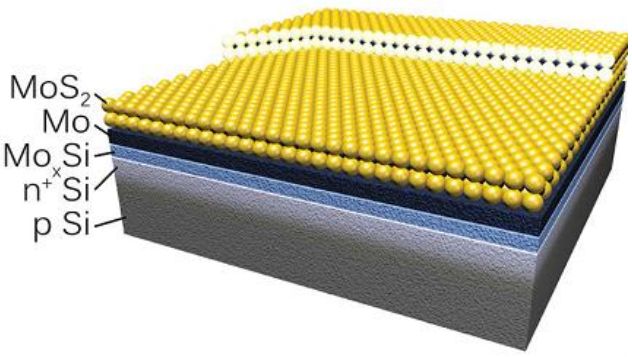

Figure 10 Diagram of MoS_2 -n^+p Si device.[78] Copyright 2014 WILEY-VCH Verlag GmbH & Co. KGaA, Weinheim

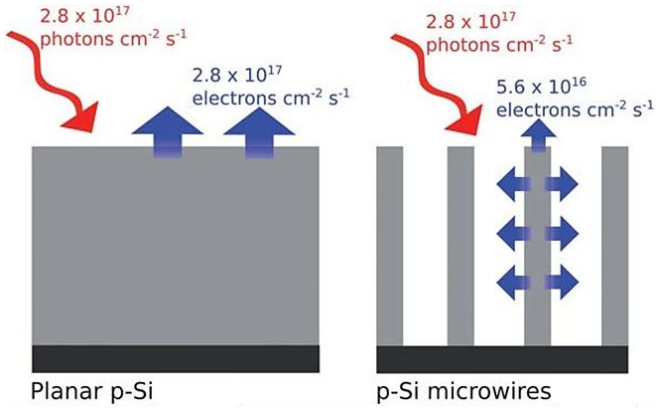

Fig.11 Relationship between the incident photon flux and outgoing electron flux in a conventional crystalline Si absorber (left) and a crystalline Si microwire array absorber (right) under AM 1.5G illumination. Assuming unity absorption above the Si bandgap and unity quantum yield for charge carrier collection, the microwire array produces a smaller electron flux per absorber surface area for the same incident photon flux.[83] Copyright 2011 The Royal Society of Chemistry.

photogenerated minority carriers is allowed and achieved respectively via the length and radial directions of the wire[84]. Because of their large semiconductor/electrolyte interfacial areas, more catalytic sites can be provided (Fig.11)[83]. Spurgeon *et al.* have grown ordered arrays of crystalline p-type silicon (p-Si) microwires on p^+-Si(111) substrate by the vapor-liquid-solid (VLS) method with Cu as catalyst on both a Si(111) substrate[85] and a flexible, optically transparent poly-dimethylsiloxane (PDMS) film[86]. However, the low photo-voltage V_{OC} of the p-Si/H_2O junction limited the energy-conversion efficiency even after adding Pt particles as co-catalyst. By introducing a buried metallurgical n^+p junction into the Si wires, the V_{OC} was increased due to the larger band bending at the n^+/p interface relative to the aqueous solution/p-Si interface[77]. Recently, in combination with a nanosphere lithography technique, Huang *et al.* reported the successful fabrication of large-area ordered Si nanowire arrays (NWAs) by a cost-effective and scalable wet-etching process[87]. Benefiting from the patterned and ordered NWs structure, an increased surface area, increased light absorption from light trapping, shortened minor carrier diffusion length, and enhanced charge transfer can be achieved. The periodical Si NWAs photocathode demonstrated a maximum photocurrent density of 27 mA/cm^2, which is ~2.5 times that of the planar Si electrode and the random Si nanowires electrode. However, even with a uniform 30 nm TiO_2 layer deposited by ALD to serve as a protection layer with no pinholes, the stability of Si wire arrays still needs to be improved. Similar to other materials covered by MoS_2, Esposito *et al.* employed a metal–insulator–semiconductor (MIS) Si-SiO_x/Ti/Pt photoelectrode architecture that allowed for stable and efficient water splitting (Fig. 12(a))[88]. The thin insulating SiO_x layer protected the semiconductor from corrosion. The holes could be blocked from the interface and the electrons could directly transfer from the semiconductor conduction band edge to the Fermi level of the metallic collector (Fig. 12(b)). The Ti/Pt bilayer

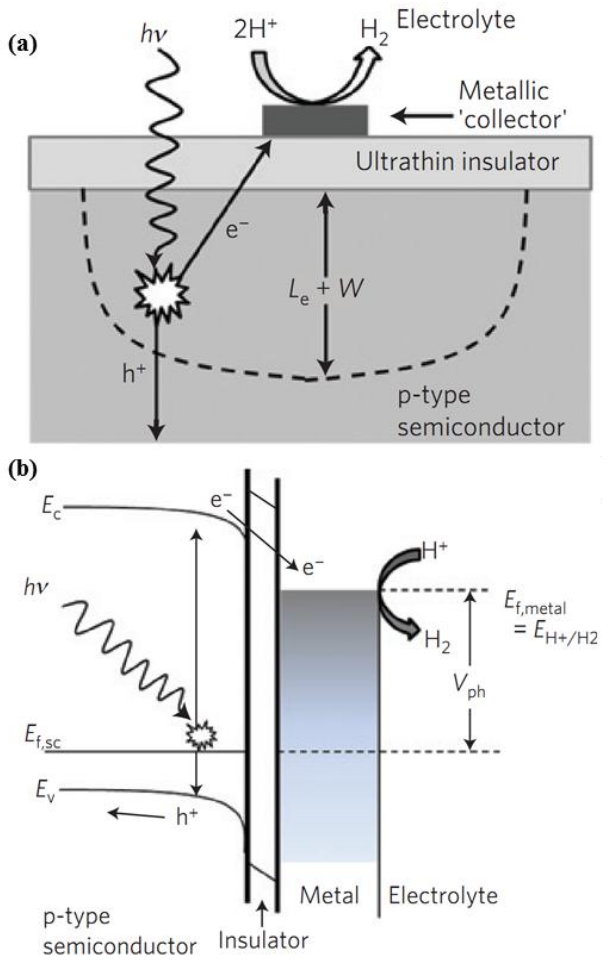

Fig.12 Conventional view of MIS photoelectrode operation. (a) Schematic side view of a MIS photoelectrode with a metallic collector situated on an insulator-covered p-type semiconductor. (b) Energy band diagram for a standard MIS photoelectrode.[88] Copyright 2013 Macmillan Publishers Limited.

structure was designed to ensure good reaction kinetics from Pt co-catalyst and a large photo-voltage from the low work function of Ti layer across the MIS junction. In this structure, a thin, negatively charged inversion layer was formed next to the Si/SiO_x interface, which enabled electrons transfer to the electrolyte. Thus, a lower recombination was achieved.

For both planar and wire Si structures, co-catalyst plays an important role at the PEC performance improvement. Dasgupta *et al.* deposited a submonolayer Pt nanoparticles as catalyst on Si NW to achieve controllable catalytic behavior at lower Pt loading level[89]. McKone *et al.* have explored the behavior of Pt, Ni and Ni-Mo co-catalysts on both planar and NWs structures of Si[83]. The electroplated Ni-Mo binary alloy particles were found to have almost the same catalytic activity as Pt on silicon photocathode. This makes the substitution of Pt by non-noble metal Ni-Mo possible.

Copper-based chalcogenides

The copper based chalcopyrites, such as the $CuIn_xGa_{1-x}Se_2$ (CIGS, 1.0 eV-1.68 eV) and kesterite Cu_2ZnSnS_4 (CZTS, 1.0 eV-

1.5 eV), have shown impressive performance in photovoltaic solar cells owe to their high absorption coefficient of ~10^5/cm, tunable direct bandgap, and high tolerance for grain boundaries[88, 90-93]. Considering choices of other chemical elements, the I-III-VI_2 chalcopyrite semiconductors (I=Cu, Ag; II=Al, In, Ga; VI=S, Se, Te) can have a wider tunable bandgap values (1.0–2.4 eV)[29, 30] and are usually p-type because of the intrinsic defects such as Cu vacancies. The chalcopyrite semiconductors have also been studied as photocathode materials in addition to their photovoltaics. In addition to CIGS, $CuGaSe_2$ (1.7eV), $CuGa_3Se_5$ (1.8 eV), and $CuInS_2$ (1.5eV) are also developed in recent years[6, 94-96]. While such photocathodes usually produce high photocurrent densities, most of them have narrow band gaps and inappropriate valence band edge and therefore are not suitable for practical solar water splitting[97].

CIGS, with high conversion efficiency in photovoltaic device, was investigated as photocathode. Yokoyama *et al.* obtained a photocurrent density of 12 mA/cm^2 at 0V vs RHE using the CdS/Pt modification[97]. The loading of CdS and Pt increased the photocurrent and stability. Jacobsson *et al.* reported a photocurrents of 6 mA/cm^2 in the configuration of a PEC cell[98]. After adding the CdS and ZnO layers (Fig.13(b)), the photocurrent was improved because the solid state p-n junction promoted charge separation and the photogenerated electrons could easily transport to the electrolyte interface (Fig.13(a)). However, the photo-corrosion of ZnO and CdS eventually hindered the performance improvement.

Another example of chalcopyrite is $CuGa_xSe_y$. Kim *et al.* showed that polycrystalline Cu-deficient $CuGaSe_2$ thin film grown via vacuum co-evaporation enlarges the bandgap with a better valence band edge for water splitting than $CuGaSe_2$[95]. However, similar to CIGS, to improve the charge separation, the p-n junction formation is a typically method to both passivate the photocathode and enhance the electron transfer

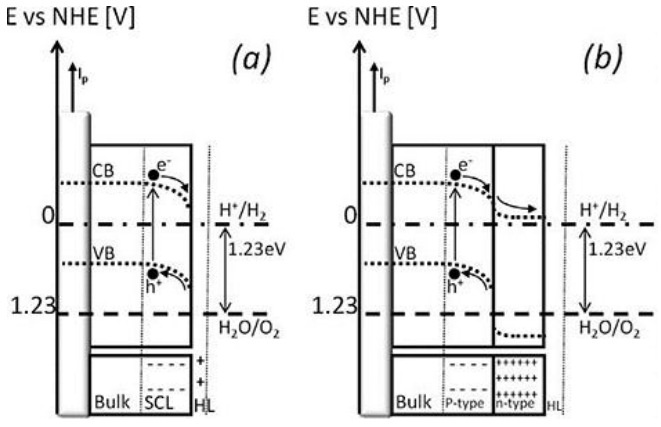

Fig. 13 (a) Energy diagram for a p-type CIGS semiconductor immersed in the electrolyte where the driving force for charge separation is the electric field created by the charge imbalance at the semiconductor/electrolyte interface. (b) The corresponding energy diagram for CIGS covered by an n-type semiconductor creating a heterogeneous p-n junction to ensure charge separation.[98] Copyright 2013, Hydrogen Energy Publications, LLC. Published by Elsevier Ltd.

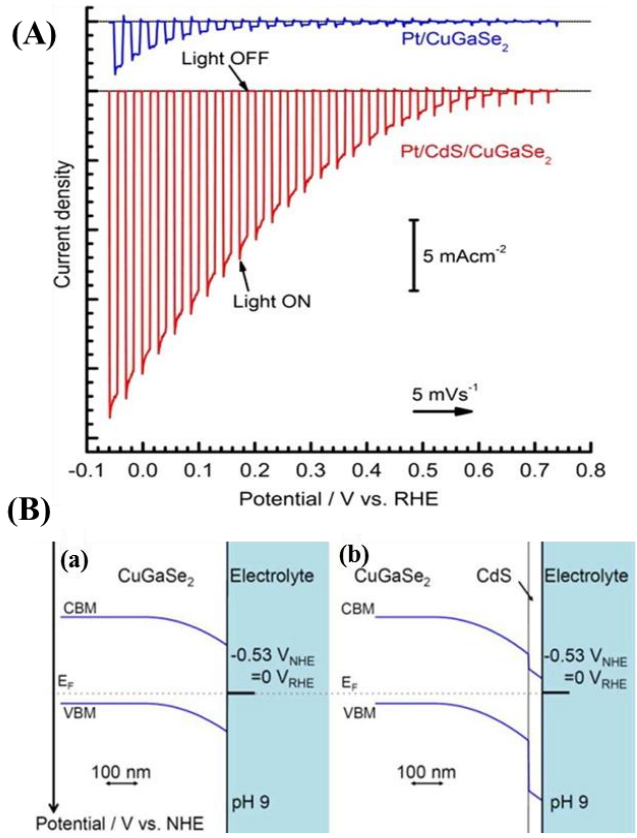

Fig. 14 (A) Current-potential curves for CGSe/Pt and CGSe /CdS/Pt electrodes [0.1M Na_2SO_4(aq), pH 9, 300 W Xe lamp, 5 mV/s]. (B) Calculated band alignment at the solid-electrolyte interfaces for (a) CGSe and (b) CGSe/CdS electrodes[99]. Copyright 2013 American Chemical Society.

to electrolyte. ZnS, CdS and ZnO, which are widely used in photovoltaic solar cell structures to improve charge separation, are also employed in PEC photocathode. Based on this, Kim *et al.* developed a copper gallium selenide ($CuGa_3Se_5$ (CGSe), Eg=1.8 eV) photocathode covered with a ZnS buffer layer via chemical bath deposition and with Pt particles as co-catalyst[95]. At 0V vs RHE, the photocurrent density from the CGSe/ZnS/Pt electrode was increased to 8.03 mA/cm^2 as compared to that of 3.04 mA/cm^2 from CGSe/Pt electrode. However, the diffusion of Zn ion through the grain boundaries may increase the n-type characteristics of CGSe photocathode. Moriya *et al.* thus used CdS to modify CGSe. A significantly increased photocurrent (Fig.14(A)) and over 20 days stability of hydrogen evolution under illumination were achieved[99]. In this structure, the CdS thin layer was completely covered by the depletion layer and the resulting cathodic polarization further increased the depletion layer and obstructed the holes from electrode to electrolyte (Fig.14(B)). More recently, Domen's group further reported a simple particle transfer method to prepared CGSe/CdS/Pt electrode. With a tunable bandgap of copper gallium selenides via various compositional ratio of Ga/Cu, they demonstrated the largest photocurrent at Ga/Cu ratio of 2[100]. By forming a p-n junction structure between $CuGa_3Se_5$ modified (Ag,Cu)$GaSe_2$ (ACGSe) and CdS, they observed a

cathodic photocurrent of 8.79 mA/cm^2 at 0 V vs RHE with over 20 days continuous hydrogen evolution[96]. Meanwhile, Gunawan *et al.* reported a Pt-In_2S_3 modified $CuInS_2$ (1.5 eV) photocathode for water splitting with the photocurrent density of about 15 mA/cm^2 at 0V vs RHE under AM 1.5G irradiation[101].

CZTS is made of chemical elements that are abundant in the earth's crust (Cu: 50 ppm, Zn: 75 ppm, Sn: 2.2 ppm, S: 260 ppm). It has recently been investigated for solar water splitting by several groups[97, 102-104]. Li *et al.* prepared the single crystalline CZTS nanosheet arrays using CuS nanosheet as sacrificial template and yielded a photocurrent density of 1.32 mA/cm^2, the highest value for the photocathode based on bare CZTS up to now, at 0V vs RHE under AM 1.5G irradiation[105].

II-VI group materials

Many of the II-VI materials are well suited for various opto-electronic applications due to their high optical absorption coefficient. Being a typical II-VI material, CdS, with a direct band gap of 2.4 eV and appropriate valence/conduction band edges for water oxidation/reduction, is one of the most promising candidate with the potential to split water without external bias[21, 28, 31]. The intrinsic CdS, which were found to be of n-type conduction as a result of the formation of the sulfur vacancies, suffered significant photo-corrosion due to its self-photo-oxidation at the photoelectrode/electrolyte interface by the photo-generated holes. Huang *et al.* successfully prepared the p-type Cu doped CdS thin film with direct band gap of 2.37 eV and high surface-to-volume ratio (Fig.15c) [106]. Hydrogen evolution from the CdS:Cu/Pt photocathode in the nearly neutral and scavenger-free electrolyte demonstrated the feasibility of using p-type CdS-based photocathode to achieve solar hydrogen production (Fig.15b). A 0.6 mA/cm^2 photocurrent of CdS:Cu/Pt photocathode was achieved (Fig. 15a).

CdTe is one of the leading materials for thin film solar cells because of its optimum band gap (1.44 eV) and the variety of thin film preparation methods. The as-prepared CdTe films are usually p-type as a result of the formation of Te vacancies. Mathew *et al.* reported the hydrogen evolution onset potential of the CdTe photocathode shifted by about 220 mV when exposed to one sun illumination and the modification with Ru improved both the stability and hydrogen evolution efficiency[107].

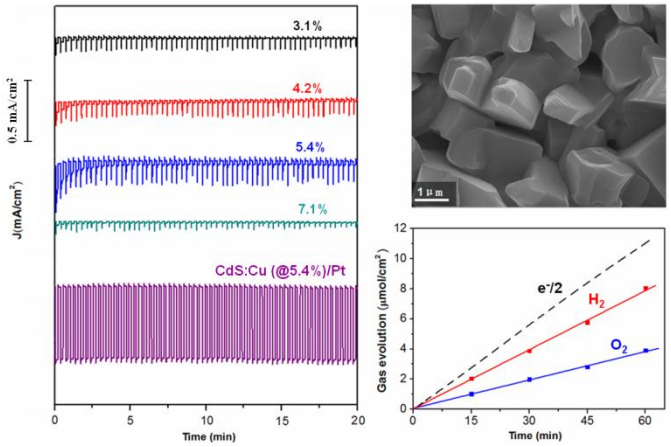

Fig. 15 (a) Current–time measurements for a number of CdS:Cu/Pt photocathodes with different Cu concentrations held at 0 V vs RHE in 1.0 M Na_2SO_4 electrolyte at pH 9 under chopped simulated AM 1.5G light. The insert is the 0.5 mA/cm^2 scale bar. (b) Evolution of hydrogen (red line) over CdS:Cu (@5.4%)/Pt at 0 V vs RHE in 1.0 M Na_2SO_4 electrolyte under simulated AM 1.5G illumination. Evolution of oxygen (blue line) over the counter electrode is plotted for comparison. The dashed black line shows ideal hydrogen evolution assuming a Faradic efficiency of 100%. (c) SEM images of CdS:Cu (@5.4%) film on Mo back contact.[106] Copyright 2014 American Chemical Society.

Conclusions and perspectives

As presented above, while great efforts have been made to search suitable photocathode materials for solar hydrogen production, up to now no good candidate is identified that can be used in practical large-scale application. Very few materials can simultaneously satisfy all the four harsh requirements as discussed previously: visible light response; appropriate conduction/valence band edges; high stability; and earth abundance with low cost.

While some materials reviewed in this feature article are from new efforts in developing semiconductor photocathodes for solar water splitting, most of them are in fact not new. Instead, the various approaches for device performance improvement, including nanostructure design, co-catalyst deposition, heterojunction formation and plasmonic effect have become the focus of research and are expected to continue in the future.

Visible light response is essential for photocathode. This determines the theoretical upper limit of energy conversion efficiency. As reviewed before, the energy conversion efficiency of the photoelectrolysis cells based on semiconductor photoelectrodes was highly limited by the light absorption efficiency. In addition to choosing the appropriate bandgap which not only provides enough electron/hole energy for water decomposition but also for overcoming the overpotentials for the respective reduction/oxidation reactions, nanostructures in photocathodes play a positive role to enhance light absorption. The optical properties of the nanostructured photocathode could be tuned via the controlled design of optical scattering and light trapping. Various nanostructures have been investigated in conjunction with the separation of the photo-excited charges. Plasmonic effects, on the other hand, have also been explored immensely for their potential applications in many different areas[108-110], including solar water splitting. The plasmonics can confine the light energy to the near-surface region of the photoelectrode as a result of both the surface plasmon resonances and photonic light trapping, and can thus decrease the required thickness of light absorbing layer to reduce the material quantity to be used and the bulk recombination of photo-

generated charge carriers. Up to now, most of the plasmonic effects investigated for water splitting were carried out on photocatalytic particles and photoanodes[111, 112]. In the future, study of the plasmonics on photocathode may attract more and more attention.

Charge separation and collection are the second factor to limit the energy conversion efficiency. Nanostructures with special shapes, such as nanowires and nanorods, can reduce the diffuse distance for the photo-excited charge carriers to transfer from their generation position to the photoelectrode/electrolyte interface, and can decouple the conflicting demands between light absorption and charge carrier transport into two different geometric directions. The higher surface/volume ratio introduced by nanostructure than the planar structure, in principle, can provide not only larger photoelectrode/electrolyte interface area but also more catalytically active sites for the redox reactions to take place. For indirect bandgap materials like Si with long light absorption length, nanostructure optimization is an effective method to solve the conflicting demand between light absorption and charge separation. Up to this point, while it has been demonstrated that nanostructures indeed could enhance light absorption and speed up charge separation, nanostructure has unfortunately not brought the promised high energy conversion efficiency, most likely because the defects introduced at the increased surface areas may function as recombination centers for photo-generated carriers. Efforts to understand the surface defects and their roles in carrier recombination in the nanostructured materials must be emphasized in the future research. Methods to avoid or passivate the negative effects brought by the nanostructure should be sought.

Deposition of heterojunction layers have been taken as another general approach to achieve fast photo-generated carrier separation via local electric field generated in the p-n junction formed between the heterojunction layer and the p-type light absorber. In terms of the photoelectrolysis, heterojunction structures have additional advantages, such as holding multiple bandgaps for better matching the solar spectrum, passivating the surface recombination centers, enhancing the chemical stability, and improving the catalytic activity of the photoelectrode surface.

The central reactions of solar water splitting are reduction/oxidization of water into hydrogen/oxygen aided with the collected photo-generated electrons/holes at the semiconductor/electrolyte interface. Even with appropriate energy band edges, most of the semiconductor materials mainly act as light absorbers but not as reactivity sites. The slow kinetics of water reduction occurred on the photocathode surfaces is normally a result from the low photo-activity of semiconductor surface which in turn induces accumulation of photo-generated electrons at the photocathode/electrolyte interface and thus self-photo-corrosion. To solve this problem, co-catalysts, which efficaciously reduce the activation energy of chemical reaction by providing alternative reaction pathways, have been widely searched to increase the activity for water reduction and lower the reaction overpotential by appropriately anchoring on to the photocathodes. In addition to the traditional noble metal co-catalysts, recently, searching less expensive earth abundant co-catalysts opened a new direction of research. Nickel and nickel-based alloys as well as MoS_x were the best studied non-noble metal catalysts for hydrogen production[18, 113-115]. To develop cheap co-catalyst for almost all the photocathode materials to make best use of the photo-generated carriers and limit the self-photo-corrosion at the semiconductor/electrolyte interface will remain to be an important direction in future photocathode study.

Stability is another critical issue in reducing the overall cost in solar hydrogen production. Unlike the photoanode, the photocathode materials may suffer from the photo-reduction corrosion when the self-reduction potential level lies more positively in NHE than the water reduction potential level. To overcome this corrosion problem, thin corrosion-resistant layers which are charge transfer allowable and kinetically stable in the corresponding electrolyte under illumination could be deposited to stabilize the photocathodes. Sometimes, this thin corrosion-resistant layer may also function as the heterojunction layer or even be catalytically active. Metal oxides have been well studied as this kind of protecting layers before, and the early design was to prepare thick layers (>100nm), which could result in good corrosion protection but with poor charge transfer[116]. Thus, ultrathin layer (tens of nanometers or even several nanometers) with good band alignment, good conductivity, and high crystalline quality should be further explored to solve this confliction between charge transfer and corrosion prevention[87, 117-120].

In future, one expects that the successful photocathode is to be made of composite material with designed structures. For visible light response and overall solar water splitting, semiconductor materials with appropriate bandgap and band edge positions should be chosen. To reduce the material usage and separate light absorption and charge separation, nanostructure designing is a good approach. To speed up charge separation, a heterojunction layer can be grown on top of the surface of the selected p-type semiconductor materials to form a p-n junction. If this heterojunction layer is not ready photo-corrosion resistive, another protection layer must be added. Such a composited and structured photocathode may be the only alternative to conquer the lack of nature-giving material and to meet all the four harsh requirements for solar water splitting as discussed above. Study on the accompanied new problems, in particular the interface and interface defects will become fundamental before we can achieve high energy conversion efficiency for the photoelectrochemical process.

Acknowledgements

This work was supported by the Theme-based Research Scheme No. T23-407/13-N of Hong Kong Research Grant Council, Focused Scheme B Grant “Center for Solar Energy Research” of the Chinese University of Hong Kong, and the National Major Science Research Program of China (Project No. 2012CB933700).

Notes and references

1. C. Gupta, *Renewable and Sustainable Energy Reviews*, 2003, **7**, 155-174.
2. Z. Peidong, Y. Yanli, Z. Yonghong, W. Lisheng and L. Xinrong, *Renewable and Sustainable Energy Reviews*, 2009, **13**, 439-449.
3. E. W. L. H. Groppe, G. S. Littell, *Oil and Gas Analysts and Forecasters*, 2006.
4. R. E. Smalley, *Mrs Bulletin*, 2005, **30**, 412-417.
5. M. G. Schultz, T. Diehl, G. P. Brasseur and W. Zittel, *Science*, 2003, **302**, 624-627.
6. B. Marsen, B. Cole and E. L. Miller, *Solar Energy Materials and Solar Cells*, 2008, **92**, 1054-1058.
7. W. D. Grossmann, I. Grossmann and K. W. Steininger, *Renewable and Sustainable Energy Reviews*, 2014, **32**, 983-993.
8. E. L. Miller, in *On Solar Hydrogen & Nanotechnology*, John Wiley & Sons, Ltd, 2010, DOI: 10.1002/9780470823996.ch1, p. 5.
9. R. van de Krol, Grätzel, Michael *Photoelectrochemical Hydrogen Production*, Springer US, 2012.
10. O. Khaselev and J. A. Turner, *Science*, 1998, **280**, 425-427.
11. S. Y. Reece, J. A. Hamel, K. Sung, T. D. Jarvi, A. J. Esswein, J. J. Pijpers and D. G. Nocera, *Science*, 2011, **334**, 645-648.
12. T. Faunce, S. Styring, M. R. Wasielewski, G. W. Brudvig, A. W. Rutherford, J. Messinger, A. F. Lee, C. L. Hill, M. Fontecave and D. R. MacFarlane, *Energy & Environmental Science*, 2013, **6**, 1074-1076.
13. A. Fujishima and K. Honda, *nature*, 1972, 37-38.
14. R. Abe, *Journal of Photochemistry and Photobiology C: Photochemistry Reviews*, 2010, **11**, 179-209.
15. F. E. Osterloh, *Chemical Society Reviews*, 2013, **42**, 2294-2320.
16. J. Augustyński, B. Alexander and R. Solarska, in *Photocatalysis*, Springer, 2011, pp. 1-38.
17. A. E. R. Mohamed and S. Rohani, *Energy Environ. Sci.*, 2011, **4**, 1065-1086.
18. A. Kudo and Y. Miseki, *Chemical Society Reviews*, 2009, **38**, 253-278.
19. W. M. d. Carvalho and F. L. Souza, *Journal of Materials Research*, 2014, **29**, 16-28.
20. J. Gan, X. Lu and Y. Tong, *Nanoscale*, 2014, **6**, 7142-7164.
21. M. G. Walter, E. L. Warren, J. R. McKone, S. W. Boettcher, Q. Mi, E. A. Santori and N. S. Lewis, *Chemical reviews*, 2010, **110**, 6446-6473.
22. Y. Lin, G. Yuan, R. Liu, S. Zhou, S. W. Sheehan and D. Wang, *Chemical Physics Letters*, 2011, **507**, 209-215.
23. N. P. Dasgupta and P. Yang, *Frontiers of Physics*, 2014, **9**, 289-302.
24. P. Zhang, L. Gao, X. Song and J. Sun, *Advanced materials*, 2015, **27**, 562-568.
25. S. Moniz, S. A. Shevlin, D. Martin, Z. Guo and J. Tang, *Energy & Environmental Science*, 2015.
26. A. Heller, E. Aharon-Shalom, W. Bonner and B. Miller, *Journal of the American Chemical Society*, 1982, **104**, 6942-6948.
27. A. Paracchino, V. Laporte, K. Sivula, M. Gratzel and E. Thimsen, *Nature materials*, 2011, **10**, 456-461.
28. W. Shangguan and A. Yoshida, *The Journal of Physical Chemistry B*, 2002, **106**, 12227-12230.
29. J. Klaer, J. Bruns, R. Henninger, K. Siemer, R. Klenk, K. Ellmer and D. Bräunig, *Semiconductor Science and Technology*, 1998, **13**, 1456.
30. A. Ennaoui, M. Bär, J. Klaer, T. Kropp, R. Sáez‐Araoz and M. C. Lux‐Steiner, *Progress in Photovoltaics: Research and Applications*, 2006, **14**, 499-511.
31. M. Grätzel, *Nature*, 2001, **414**, 338-344.
32. Q. Huang, F. Kang, H. Liu, Q. Li and X. Xiao, *J. Mater. Chem. A*, 2013, **1**, 2418-2425.
33. Q. Yu, X. Meng, T. Wang, P. Li, L. Liu, K. Chang, G. Liu and J. Ye, *Chemical communications*, 2015, **51**, 3630-3633.
34. M. S. Prevot, N. Guijarro and K. Sivula, *ChemSusChem*, 2015, **8**, 1359-1367.
35. U. A. Joshi, 2014, **174**, 97-112.
36. U. A. Joshi and P. A. Maggard, *The Journal of Physical Chemistry Letters*, 2012, **3**, 1577-1581.
37. Y. Matsumoto, M. Omae, K. Sugiyama and E. Sato, *Journal of Physical Chemistry*, 1987, **91**, 577-581.
38. W. H. Baur, *Journal of Solid State Chemistry*, 1982, **43**, 222-224.
39. K. L. Sowers and A. Fillinger, *Journal of The Electrochemical Society*, 2009, **156**, F80.
40. Z. Liu, Z.-G. Zhao and M. Miyauchi, *The Journal of Physical Chemistry C*, 2009, **113**, 17132-17137.
41. J. Nian, C. Hu and H. Teng, *International Journal of Hydrogen Energy*, 2008, **33**, 2897-2903.
42. P. De Jongh, D. Vanmaekelbergh and J. J. d. Kelly, *Journal of The Electrochemical Society*, 2000, **147**, 486-489.
43. L. Wu, L.-k. Tsui, N. Swami and G. Zangari, *The Journal of Physical Chemistry C*, 2010, **114**, 11551-11556.
44. C. Yang, P. D. Tran, P. P. Boix, P. S. Bassi, N. Yantara, L. H. Wong and J. Barber, *Nanoscale*, 2014, **6**, 6506-6510.
45. Z. H. Zhang and P. Wang, *J Mater Chem*, 2012, **22**, 2456-2464.
46. A. Paracchino, J. C. Brauer, J.-E. Moser, E. Thimsen and M. Graetzel, *The Journal of Physical Chemistry C*, 2012, **116**, 7341-7350.
47. T. D. Golden, M. G. Shumsky, Y. Zhou, R. A. VanderWerf, R. A. Van Leeuwen and J. A. Switzer, *Chemistry of Materials*, 1996, **8**, 2499-2504.
48. R. S. Toth, R. Kilkson and D. Trivich, *Journal of Applied Physics*, 1960, **31**, 1117.
49. K. S. Joya, Y. F. Joya, K. Ocakoglu and R. van de Krol, *Angewandte Chemie International Edition*, 2013, **52**, 10426-10437.
50. S. Choudhary, S. Upadhyay, P. Kumar, N. Singh, V. R. Satsangi, R. Shrivastav and S. Dass, *international journal of hydrogen energy*, 2012, **37**, 18713-18730.
51. A. Paracchino, N. Mathews, T. Hisatomi, M. Stefik, S. D. Tilley and M. Grätzel, *Energy & Environmental Science*, 2012, **5**, 8673.
52. J. Han, X. Zong, X. Zhou and C. Li, *RSC Adv.*, 2015, **5**, 10790-10794.
53. B. C. Steele and A. Heinzel, *Nature*, 2001, **414**, 345-352.
54. H. Tanaka, M. Taniguchi, M. Uenishi, N. Kajita, I. Tan, Y. Nishihata, J. i. Mizuki, K. Narita, M. Kimura and K. Kaneko, *Angewandte Chemie*, 2006, **118**, 6144-6148.
55. Q. Liu, K.-d. Wang and X.-d. Xiao, *Frontiers of Physics in China*, 2010, **5**, 357-368.
56. P. D. Tran, L. H. Wong, J. Barber and J. S. Loo, *Energy & Environmental Science*, 2012, **5**, 5902-5918.

57. X. Guo, P. Diao, D. Xu, S. Huang, Y. Yang, T. Jin, Q. Wu, M. Xiang and M. Zhang, *International Journal of Hydrogen Energy*, 2014, **39**, 7686-7696.
58. C. G. Morales-Guio, L. Liardet, M. T. Mayer, S. D. Tilley, M. Gratzel and X. Hu, *Angewandte Chemie*, 2015, **54**, 664-667.
59. C. G. Morales-Guio, S. D. Tilley, H. Vrubel, M. Gratzel and X. Hu, *Nature communications*, 2014, **5**, 3059.
60. X. Zhao, P. Wang, Z. Yan and N. Ren, *Chemical Physics Letters*, 2014, **609**, 59-64.
61. S. Ida, K. Yamada, T. Matsunaga, H. Hagiwara, Y. Matsumoto and T. Ishihara, *Journal of the American Chemical Society*, 2010, **132**, 17343-17345.
62. K. Sekizawa, T. Nonaka, T. Arai and T. Morikawa, *ACS applied materials & interfaces*, 2014, **6**, 10969-10973.
63. O. Palasyuk, A. Palasyuk and P. A. Maggard, *Inorganic chemistry*, 2010, **49**, 10571-10578.
64. I. Sullivan, P. P. Sahoo, L. Fuoco, A. S. Hewitt, S. Stuart, D. Dougherty and P. A. Maggard, *Chemistry of Materials*, 2014, **26**, 6711-6721.
65. S. S. Kocha and J. A. Turner, *Journal of the Electrochemical Society*, 1995, **142**, 2625-2630.
66. J. Kamimura, P. Bogdanoff, J. Lahnemann, C. Hauswald, L. Geelhaar, S. Fiechter and H. Riechert, *Journal of the American Chemical Society*, 2013, **135**, 10242-10245.
67. S. Licht, B. Wang, S. Mukerji, T. Soga, M. Umeno and H. Tributsch, *The Journal of Physical Chemistry B*, 2000, **104**, 8920-8924.
68. C. Liu, J. Sun, J. Tang and P. Yang, *Nano letters*, 2012, **12**, 5407-5411.
69. M. H. Lee, K. Takei, J. Zhang, R. Kapadia, M. Zheng, Y. Z. Chen, J. Nah, T. S. Matthews, Y. L. Chueh, J. W. Ager and A. Javey, *Angewandte Chemie*, 2012, **51**, 10760-10764.
70. L. Gao, Y. Cui, J. Wang, A. Cavalli, A. Standing, T. T. Vu, M. A. Verheijen, J. E. Haverkort, E. P. Bakkers and P. H. Notten, *Nano letters*, 2014, **14**, 3715-3719.
71. J. M. Foley, M. J. Price, J. I. Feldblyum and S. Maldonado, *Energy Environ. Sci.*, 2012, **5**, 5203-5220.
72. A. I. Hochbaum and P. Yang, *Chemical reviews*, 2009, **110**, 527-546.
73. S. S. Kocha, J. A. Turner and A. J. Nozik, *Journal of Electroanalytical Chemistry*, 1994, **367**, 27-30.
74. S. Fan, B. AlOtaibi, S. Y. Woo, Y. Wang, G. A. Botton and Z. Mi, *Nano letters*, 2015, **15**, 2721-2726.
75. J. Wu, Y. Li, J. Kubota, K. Domen, M. Aagesen, T. Ward, A. Sanchez, R. Beanland, Y. Zhang, M. Tang, S. Hatch, A. Seeds and H. Liu, *Nano letters*, 2014, **14**, 2013-2018.
76. C. Maier, M. Specht and G. Bilger, *International journal of hydrogen energy*, 1996, **21**, 859-864.
77. S. W. Boettcher, E. L. Warren, M. C. Putnam, E. A. Santori, D. Turner-Evans, M. D. Kelzenberg, M. G. Walter, J. R. McKone, B. S. Brunschwig, H. A. Atwater and N. S. Lewis, *Journal of the American Chemical Society*, 2011, **133**, 1216-1219.
78. J. D. Benck, S. C. Lee, K. D. Fong, J. Kibsgaard, R. Sinclair and T. F. Jaramillo, *Advanced Energy Materials*, 2014, **4**, n/a-n/a.
79. Y. W. Chen, J. D. Prange, S. Dühnen, Y. Park, M. Gunji, C. E. Chidsey and P. C. McIntyre, *Nature materials*, 2011, **10**, 539-544.
80. A. Kargar, J. S. Cheung, C. H. Liu, T. K. Kim, C. T. Riley, S. Shen, Z. Liu, D. J. Sirbuly, D. Wang and S. Jin, *Nanoscale*, 2015, **7**, 4900-4905.
81. M. J. Choi, J.-Y. Jung, M.-J. Park, J.-W. Song, J.-H. Lee and J. H. Bang, *Journal of Materials Chemistry A*, 2014, **2**, 2928.
82. Q. Ding, F. Meng, C. R. English, M. Caban-Acevedo, M. J. Shearer, D. Liang, A. S. Daniel, R. J. Hamers and S. Jin, *Journal of the American Chemical Society*, 2014, **136**, 8504-8507.
83. J. R. McKone, E. L. Warren, M. J. Bierman, S. W. Boettcher, B. S. Brunschwig, N. S. Lewis and H. B. Gray, *Energy & Environmental Science*, 2011, **4**, 3573.
84. B. M. Kayes, H. A. Atwater and N. S. Lewis, *Journal of applied physics*, 2005, **97**, 114302.
85. S. W. Boettcher, J. M. Spurgeon, M. C. Putnam, E. L. Warren, D. B. Turner-Evans, M. D. Kelzenberg, J. R. Maiolo, H. A. Atwater and N. S. Lewis, *Science*, 2010, **327**, 185-187.
86. J. M. Spurgeon, S. W. Boettcher, M. D. Kelzenberg, B. S. Brunschwig, H. A. Atwater and N. S. Lewis, *Advanced materials*, 2010, **22**, 3277-3281.
87. S. Huang, H. Zhang, Z. Wu, D. Kong, D. Lin, Y. Fan, X. Yang, Z. Zhong, S. Huang and Z. Jiang, *ACS applied materials & interfaces*, 2014, **6**, 12111-12118.
88. D. V. Esposito, I. Levin, T. P. Moffat and A. A. Talin, *Nature materials*, 2013, **12**, 562-568.
89. N. P. Dasgupta, C. Liu, S. Andrews, F. B. Prinz and P. Yang, *Journal of the American Chemical Society*, 2013, **135**, 12932-12935.
90. P. Jackson, D. Hariskos, E. Lotter, S. Paetel, R. Wuerz, R. Menner, W. Wischmann and M. Powalla, *Progress in Photovoltaics: Research and Applications*, 2011, **19**, 894-897.
91. D. A. R. Barkhouse, O. Gunawan, T. Gokmen, T. K. Todorov and D. B. Mitzi, *Progress in Photovoltaics: Research and Applications*, 2012, **20**, 6-11.
92. T. K. Todorov, K. B. Reuter and D. B. Mitzi, *Advanced materials*, 2010, **22**, E156-E159.
93. T. J. Jacobsson, V. Fjällström, M. Edoff and T. Edvinsson, *Solar Energy Materials and Solar Cells*, 2015, **134**, 185-193.
94. F. Liu, Y. Li, K. Zhang, B. Wang, C. Yan, Y. Lai, Z. Zhang, J. Li and Y. Liu, *Solar Energy Materials and Solar Cells*, 2010, **94**, 2431-2434.
95. J. Kim, T. Minegishi, J. Kobota and K. Domen, *Energy Environ. Sci.*, 2012, **5**, 6368-6374.
96. L. Zhang, T. Minegishi, M. Nakabayashi, Y. Suzuki, K. Seki, N. Shibata, J. Kubota and K. Domen, *Chem. Sci.*, 2015, **6**, 894-901.
97. D. Yokoyama, T. Minegishi, K. Jimbo, T. Hisatomi, G. Ma, M. Katayama, J. Kubota, H. Katagiri and K. Domen, *Applied Physics Express*, 2010, **3**, 101202.
98. T. J. Jacobsson, C. Platzer-Björkman, M. Edoff and T. Edvinsson, *International Journal of Hydrogen Energy*, 2013, **38**, 15027-15035.
99. M. Moriya, T. Minegishi, H. Kumagai, M. Katayama, J. Kubota and K. Domen, *Journal of the American Chemical Society*, 2013, **135**, 3733-3735.
100. H. Kumagai, T. Minegishi, Y. Moriya, J. Kubota and K. Domen, *The Journal of Physical Chemistry C*, 2014, **118**, 16386-16392.
101. Gunawan, W. Septina, S. Ikeda, T. Harada, T. Minegishi, K. Domen and M. Matsumura, *Chemical communications*, 2014, **50**, 8941.

102. J. J. Scragg, P. J. Dale and L. M. Peter, *Electrochemistry Communications*, 2008, **10**, 639-642.
103. H. Katagiri, K. Jimbo, W. S. Maw, K. Oishi, M. Yamazaki, H. Araki and A. Takeuchi, *Thin Solid Films*, 2009, **517**, 2455-2460.
104. L. Rovelli, S. D. Tilley and K. Sivula, *ACS applied materials & interfaces*, 2013, **5**, 8018-8024.
105. B.-J. Li, P.-F. Yin, Y.-Z. Zhou, Z.-M. Gao, T. Ling and X.-W. Du, *RSC Adv.*, 2015, **5**, 2543-2549.
106. Q. Huang, Q. Li and X. Xiao, *The Journal of Physical Chemistry C*, 2014, **118**, 2306-2311.
107. X. Mathew, A. Bansal, J. Turner, R. Dhere, N. Mathews and P. Sebastian, *Journal of New Materials for Electrochemical Systems*, 2002, **5**, 149-154.
108. C.-H. Chou and F.-C. Chen, *Nanoscale*, 2014, **6**, 8444-8458.
109. O. Tokel, F. Inci and U. Demirci, *Chemical reviews*, 2014, **114**, 5728-5752.
110. C. Wang and D. Astruc, *Chemical Society Reviews*, 2014, **43**, 7188-7216.
111. H. M. Chen, C. K. Chen, R.-S. Liu, L. Zhang, J. Zhang and D. P. Wilkinson, *Chemical Society Reviews*, 2012, **41**, 5654-5671.
112. S. C. Warren and E. Thimsen, *Energy & Environmental Science*, 2012, **5**, 5133-5146.
113. H. Kato, K. Asakura and A. Kudo, *Journal of the American Chemical Society*, 2003, **125**, 3082-3089.
114. S. Ikeda, M. Hara, J. N. Kondo, K. Domen, H. Takahashi, T. Okubo and M. Kakihana, *Chemistry of materials*, 1998, **10**, 72-77.
115. C. G. Morales‐Guio, L. Liardet, M. T. Mayer, S. D. Tilley, M. Grätzel and X. Hu, *Angewandte Chemie International Edition*, 2015, **54**, 664-667.
116. P. A. Kohl, S. N. Frank and A. J. Bard, *Journal of The Electrochemical Society*, 1977, **124**, 225-229.
117. L. Guo, D. Hung, W. Wang, W. Shen, L. Zhu, C.-L. Chien and P. C. Searson, *Applied Physics Letters*, 2010, **97**, 063111.
118. K. H. Yoon, C. W. Shin and D. H. Kang, *Journal of applied physics*, 1997, **81**, 7024-7029.
119. Z. Zhang, R. Dua, L. Zhang, H. Zhu, H. Zhang and P. Wang, *Acs Nano*, 2013, **7**, 1709-1717.
120. L. Ji, M. D. McDaniel, S. Wang, A. B. Posadas, X. Li, H. Huang, J. C. Lee, A. A. Demkov, A. J. Bard and J. G. Ekerdt, *Nature nanotechnology*, 2015, **10**, 84-90.

Table of Contents

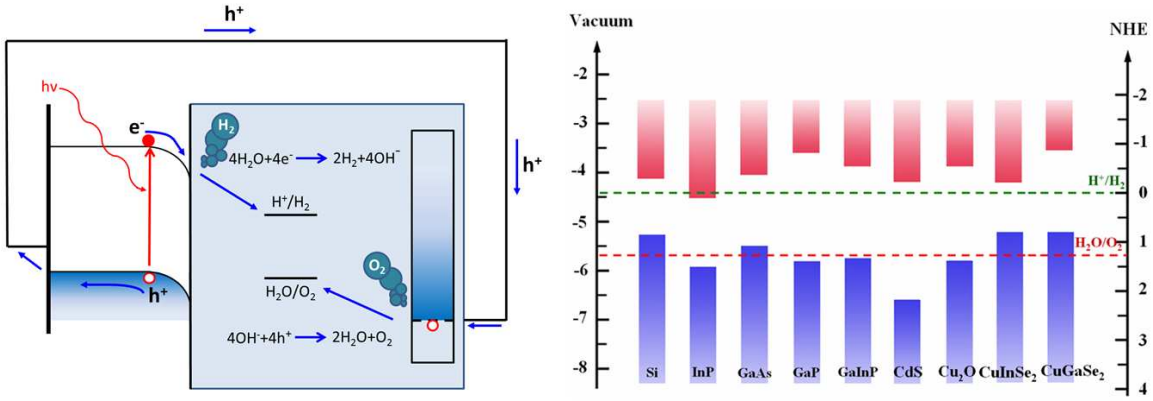

Recent efforts to improve the performance of photocathodes for hydrogen evolution were reviewed.